DFT investigation of strong acceptor molecules

Aqeel Mohsin Ali

Polymer Research Center, University of Basrah, Basrah, Iraq

aqeel.mohsin@uobasrah.edu.iq

Received 15 Sep. 2024, Accepted 13 May. 2025, Published 30 June. 2025.

DOI: 10.52113/2/12.01.2025/176-183

Abstract: This paper describes the creation of three near-infrared (NIR) acceptors, namely BCDT, BCDT-4F, and BCDT-4Cl, with the A−D−C−D−A (acceptor−donor−core−donor−acceptor)-type conformation. The acceptors use intramolecular noncovalent interactions to ensure the conservation of the molecular shape of the unfused complexes. Quantifications of E_{HOMO}, E_{LUMO}, Eg, λ_{max}, E_x, and ESP have been calculated to illustrate the optoelectronic and structure-related properties. In the gas phase, the non-fullerene acceptor BCDT-4Cl has shown the lowest band gap energy of 1.87 eV and the lowest excitation energy of 1.66 eV. Thus, it is anticipated that BCDT-4Cl will emerge as a very viable candidate for future organic non-fullerene acceptors. We have calculated the dipole moments of the specified acceptors for both the ground state (μ_g) and the excited state (μ_e). Notably, BCDT-4Cl had the highest dipole moment values, namely μ_g = 5.66 and μ_e = 6.86 Debye. The predicted λ_{max} value of 734 nm obtained by Density Functional Theory (DFT) for the reference molecule is consistent with the actual λ_{max} value of 784 nm. The synthesised compounds have acute sensitivity in the near-infrared region and show a red shift in the absorption spectra, therefore covering a broader spectrum of wavelengths ranging from 730 to 7743 nm.

***Keywords*:** DFT, Near infrared acceptor, Solar cell, Absorption spectrum, Molecular orbitals, Dipole moment.

1. Introduction

Recently, single-junction organic solar cells (OSCs) have achieved power conversion efficiencies (PCEs) over 17%, indicating their outstanding progress.[1] Considerable work has been dedicated to investigating novel nonfullerene acceptors (NFAs), which possess both easily modifiable optoelectronic characteristics and simpler synthetic intricacies.[2,3]

The amplification of the charge carrier transfer belong molecular skeleton action is necessary to expand the light absorption toward wavelengths in the range of near-infrared (NIR). This is essential for achieving large current and, therefore, high power conversion efficiencies (PCEs) in organic solar cells (OSCs). [4,5] Furthermore, the process of halogenation of the molecular skeleton is also efficient in the development of near-infrared acceptors. This is because halogen atoms have the ability to improve both the effects of intermolecular contact (ICT) and intermolecular interactions. [6-8] To date, numerous strong acceptors exhibiting crucial execution in solar cells are

showcased through the incorporation of halogen atoms into the structure. Moreover, the synthesis of these multiring fused ladder structures involves intricate steps, resulting in a low overall yield and elevated material costs. Extra works are essential to investigate the chemical modelling that enables both the precise adjustment of optoelectronic properties and the reduction of the synthetic complexities associated with NFAs. Recently, C. He team published findings on several effective NFAs.[9] In the meantime, the chemical units can be readily adjusted to optimize the optoelectronic properties of the designed acceptors. This modelling plan has the potential to significantly streamline the synthetic processes and lower expenses. In contrast to the electron-donating cores previously utilized (such as benzene and thiophene) for the development of NFAs, they present acceptors that incorporate the electron-soft unit in the middle of molecule. Using ab-initio first principle computational methods, this work systematically investigates optimal structures, molecular energy levels, and the electron excitation spectrum.

2. Methodology

Acceptor molecules are studied structurally, electrically, and optically by means of density functional theory (DFT) computations. To find out how the doping were altered the molecules, we ran ground-state calculations. Equations for the ground state included the energy gap, the energy of molecular orbitals, and the optical spectra were examined. To get an idea of all the important features of the ground state, we used a density functional theory program. Finding the UV-visible spectra using time-dependent density functional theory (TD-DFT) also helped in determining the highest wavelength of absorption. Geometry optimization was initially performed on the acceptor molecule BCDT, BCDT-4F, and BCDT-4Cl which closely resembles the standard as shown in figure 1. This was achieved using B3LYP functional with 6-31G (d) basis set. This method is employed for the optimization, electronic energy states and optical properties. Gaussview 5.0 suite facilitated the prediction of

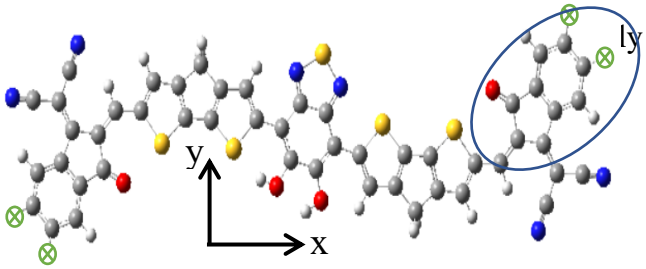

Fig. 1: The chemical structure of BCDT. Carbon (grey), sulfur (yellow), nitrogen (blue), hydrogen (white), doping site of Cl and F atoms (⊗). Acceptor group in elliptic.

3. Results and Discussion

The bond length and BLA values for the acceptor group as shown in figure 2 in all three systems are represented in Table 1. In the center

of the spectrum between C-C bonds (1.54 Å) and C=C bonds (1.33 Å) are bond length values ranging from 1.381 to 1.489 Å. Consequently, a few of the bonds that were measured do not qualify as single or double bonds. Since all of the molecules in BCDT-4Cl are acceptable

acceptors, the BLA values are somewhat lower than those of BCDT-4F but noticeably higher than those of BCDT. In addition, bigger BLA means lower energy levels and bigger bond disparities. A possible explanation for why BCDT-4F and BCDT-4Cl have somewhat greater BLA values than BCDT is that they are more likely to have a lower LUMO level.

The dipole moment values for the acceptor systems are represented in table 2. The dipole components in X and Z directions increase for fluorinated and chlorinated terminal group, while the dipole component in Y direction is lowered. The total values of dipole moment increase for fluorinated and chlorinated terminal group, and according to the findings, intermolecular interactions are greater with a chlorinated terminal group compared to a fluorinated one. These results may explain the experimental findings that fluorinated and chlorinated terminal group exhibits enhanced J aggregation and tighter molecular packing, resulting in an optimal blend morphology when combined with the polymer donor.[9]

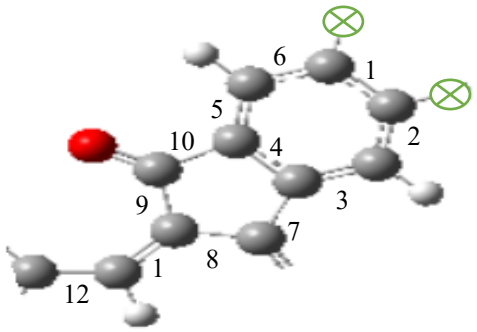

Fig. 2: The bonds in acceptor group in BCDT.

Table 1. The bond length and BLA of acceptor group.

Bond length (Å)	Acceptor		
	BCDT	BCDT-4F	BCDT-4Cl
1	1.39993	1.40261	1.40861
2	1.39911	1.38948	1.40024
3	1.39977	1.40081	1.39633
4	1.40692	1.40589	1.40485
5	1.38781	1.38913	1.38413
6	1.39652	1.38666	1.39635
7	1.48889	1.48680	1.48801
8	1.46500	1.46673	1.46630
9	1.47890	1.47842	1.47776
10	1.48014	1.47923	1.48060
11	1.38243	1.38067	1.38186
12	1.41522	1.41686	1.41570
BLA	0.06956	0.07204	0.07001

Table 2. The dipole moments of acceptors.

Dipole moment (Debye)	Acceptor		
	BCDT	BCDT-4F	BCDT-4Cl
X	4.85	5.00	5.12
Y	0.79	0.64	0.50
Z	0.93	2.11	2.36
Total	5.00	5.47	5.66

Investigating the frontier molecular orbitals (FMOs) is beneficial for understanding the optical and electrical characteristics of compounds BCDT, BCDT-4F and BCDT-

4Cl.[9] Density functional theory was used to optimize these designed compounds at B3LYP 6-31G (d). The E_{HOMO}, E_{LUMO} energies and band gap of these three compounds are shown in table 3. The molecule BCDT-4F has the lowest energy of the E_{HOMO} at -5.82 eV, while the BCDT molecule has the highest energy at -5.35 eV. The energy gaps (E_g) are regarded as a crucial characteristic as lower E_g values facilitate excitation, thereby enhancing the photoexcitation phenomena. Molecular structures BCDT and BCDT-4Cl have the lowest energy gap (E_g) values of 1.91 and 1.87 eV, respectively, while BCDT-4F has the greatest E_g value of 2.23 eV among the proposed acceptors.

Table 3. The calculated orbital and band gap energies of acceptors at B3LYP/6-31 G(d) in gas phase.

Acceptor	E_{HOMO} (eV)	E_{LUMO} (eV)	E_g (eV)
BCDT	-5.35	-3.45	1.91
BCDT-4F	-5.82	-3.59	2.23
BCDT-4Cl	-5.53	-3.66	1.87

Delocalization of electronic density may be inferred from the distribution of occupied and empty orbitals in molecules as shown in figure 3. There exists a clear correlation between the band-gap energy and the molecular structure. Enhanced conjugation with a more planar shape of the molecule is associated with a reduction in band-gap energy. The three molecules exhibit planar geometry and prolonged conjugation. As shown by C. He et al. that the molecules BCDT-4F and BCDT-4Cl exhibited the lowest energy conformation when subjected to a torsion angle 0º. [9] Consequently, BCDT-4Cl molecule provides the lowest E_g value of 1.87 eV. Nevertheless, the acceptor moiety of BCDT-4F resulted in higher E_g value of 2.23 eV. This may be attributed to the decreased conjugation seen in the molecules that caused by different electronegativity of chlorine and fluorine atoms (3.16 and 3.98 respectively).

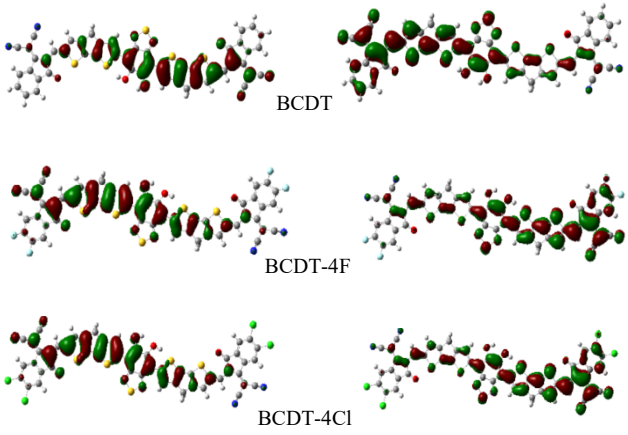

Fig. 3. Distribution of HOMO and LUMO of the acceptor molecules.

The dipole moments values of BCDT, BCDT-4F and BCDT-4Cl molecules, both in their optimized geometry (μ_g) and in the excited state (μ_e), were computed in the gas phase. Table 4 presents the values for μ_g, μ_e, and the difference

$\mu_e - \mu_g$. The dipole moment serves as a critical parameter for molecules. Compounds exhibiting elevated dipole moments may demonstrate increased charge separation. The increased charge separation enhances the molecule's ability to adjust excited electrons. The significant dipole moment facilitates the straightforward manufacture of the bulk-heterojunction.

The calculated μ_e indicating a notable difference in their measurements. In a comparable manner, the elevated values of μ_e–μ_g indicate that the transition state exhibits significant polarity in comparison to the ground state. The μ_e values for BCDT, BCDT-4F and BCDT-4Cl are 5.00, 5.46, and 5.66 Debye, while their ground state (μ_g) values fall within the range of 6.38–6.86 Debye. The μ_e–μ_g values are 1.22, 1.38, and 3.2 Debye. The minimum value of μ_e–μ_g for BCDT-4Cl indicates that the excited state exhibits a slightly greater polarity compared to the ground state. This suggests that the BCDT molecules are likely to exhibit greater efficiency in the fabrication process via solution-processed bulk heterojunction.

Table 4. The ground state ($\boldsymbol{\mu_g}$) and excited state dipole moments ($\boldsymbol{\mu_e}$) in gas phase.

Acceptor	μ_g	μ_e	$\mu_e - \mu_g$
BCDT	5.00	6.38	1.38
BCDT-4F	5.46	6.75	1.29
BCDT-4Cl	5.66	6.86	1.22

The UV-VIS investigation was performed using B3LYP 6-31G (d). The optical properties were determined for the designed molecules in the gas phase. Table 5 presents λ_{max}, excitation energies (Ex) associated with the first excited state, oscillator strength (f), and the percentage contribution of HOMO to LUMO in major transition. The λ_{max} values exhibit a red shift in the following sequence: BCDT-4Cl > BCDT-4F > BCDT. The rise in λ_{max} can be linked to the presence of extended conjugation within the molecule, that particularly attributed to the bridge of whole molecules, has the potential to improve the efficiency of solar cells. The extended conjugation decreases the LUMO energy, leading to a lower band-gap and a red shift in λ_{max} values.

The observed red shift in the λ_{max} value, combined with significant light absorption, has led to a reduction in excitation energy, thereby enhancing the electron-acceptor characteristics of the molecules. The incorporation of F and Cl atoms extended conjugation within the acceptor molecules led to the highest observed λ_{max} value of 734 and 743 nm, respectively. The E_x-value offers significant insights regarding the excitation process of an electron transitioning from the valence band (HOMO) to the conduction band (LUMO). A reduced value of E_x facilitates the process of excitation. Table 5 indicates that the sequence of E_x values is BCDT, followed by BCDT-4F, then BCDT-4Cl. The BCDT exhibits the highest value at 1.69 eV,

whereas BCDT-4F and BCDT-4Cl present the lowest value of 1.68 and 1.66 eV, respectively. The assignment of HOMO to LUMO to have the same major transition contribution of about 70%. The oscillation factor (f) ranges from 2.26 to 2.33 for molecules, which indicated to a charge transfer operation occur within the electron excitation process. All the designed acceptor molecules exhibited excitation energies (E_x) that were lower than the ground state band-gap energies (E_g). This trend aligns with previously reported data regarding the E_x and E_g values.

Table 5. The optical parameters of molecules. Values in parenthesis are experimental results.[9]

cceptor	λ_{max} (nm)	E_g^{opt} (eV)	f	Major transition
BCDT	730	1.69	2.30	HOMO-LUMO 70%
BCDT-4F	734 (784)	1.68 (1.40)	2.26	HOMO-LUMO 70%
BCDT-4Cl	743 (806)	1.66 (1.38)	2.33	HOMO-LUMO 70%

Using TD-DFT/B3LYP 6-31G (d), the absorption spectra are shown in Figure 4. A like pattern may be seen in the gas phase, with the exception of the fact that the λ_{max} of all molecules exhibits a little red shift. On the other hand, the proposed acceptor BCDT-4Cl was shown to have the lowest absorption excitation energy. It is possible to ascribe the prolonged conjugation that occurs as a result of the presence of the chlorine atoms to the fact that BCDT-4Cl has the maximum absorption capability. In the gas phase, the sequence of the maximum wavelength values for various molecules is as follows: BCDT > BCDT-4F > BCDT-4Cl.

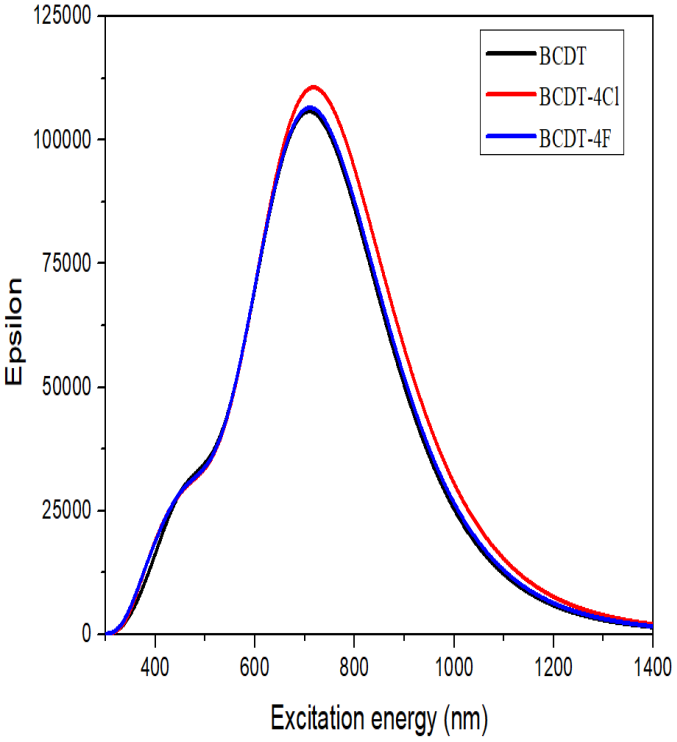

Fig. 4. The optical spectra of molecules.

Electrostatic potential (ESP) is a technique that use three-dimensional visualization to illustrate the distribution of charges across a molecule. It also calls attention to the many sites inside the molecule where electrons may be located. For the purpose of making a forecast about the reactive potential of molecular frameworks, an ESP analysis was performed on the molecules that were under consideration as shown in figure 5. The electrostatic potential maps illustrate the

three-dimensional distribution of electrons, lone pairs, and electronegative substances that are easily accessible for nucleophilic activity. When looking at the ESP maps, a region that is red implies that it has a high concentration of electrons. An area with a low concentration of electrons is represented by the color blue, whereas a region that is neutral is represented by the color green. The color maps for the BCDT, BCDT-4F and BCDT-4Cl ESP applications are shown in Figure 5. The N and O atoms that are located in the outer acceptor molecular areas are shown as having a deep red color on ESP maps. This is because of the high electron density that exists above these places. In a similar manner, the oxygen atoms that are located in the acceptor area of the core appear in red, which makes it immediately apparent that there is an electron density in those places.

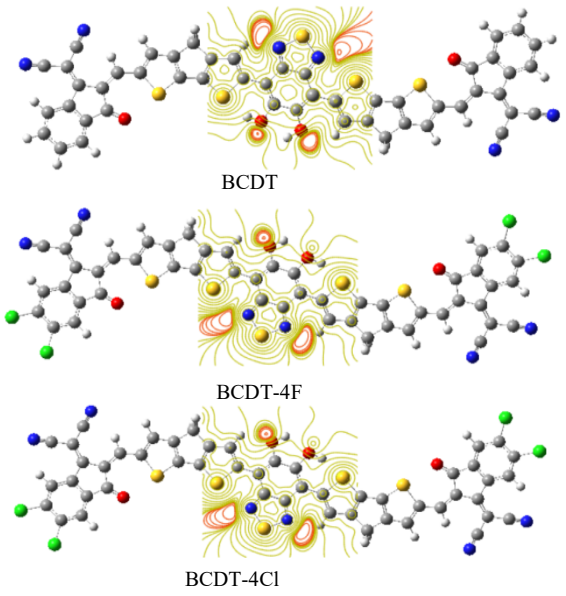

Fig. 5: The ESP map of molecules.

4. Conclusion

The design of three near-infrared (NIR) acceptors, BCDT, BCDT-4F and BCDT-4Cl, are described. The frontier energy molecular states, energy gap, electronic excitation properties and electrostatic potential map quantities have been computed to demonstrate the optoelectronic and structure-related characteristics. The acceptor BCDT-4Cl developed has shown the lowest band gap energy and excitation energy in the gas phase of 1.66 eV. Therefore, it is expected that BCDT-4Cl will be a promising contender for future organic non-fullerene acceptors. The computed dipole moments of the designed acceptors have been determined for both the ground state and the excited state. Among them, BCDT-4Cl exhibited the greatest dipole moment values. The wavelength of maximum excited state values are in the visible region. The developed compounds exhibit near-infrared sensitivity and display a red shift in the absorption spectra.

References

[1] Hou, J., Inganäs, O., Friend, R. H. and Gao, F. “Organic Solar Cells Based on Non-Fullerene Acceptors” Natural Materials. Vol. 17, pp. 119−128, 2018.

[2] Cheng, P., Li, G., Zhan, X. and Yang, Y. “Next-Generation Organic Photovoltaics Based on Non-Fullerene Acceptors” Natural Photonics, Vol. 12, pp. 131−142, 2018.

[3] Liu, S., Yuan, J., Deng, W., Luo, M., Xie, Y., Liang, Q., Zou, Y., He, Z., Wu, H. and Cao, Y. “High-Efficiency Organic Solar Cells with

Low Non-Radiative Recombination Loss and Low Energetic Disorder" Natural Photonics, 2020.

[4] Rafiq, A., Hussain, R., Khan, M.U., Mehboob, M.Y., Khalid, M., Alam, M.M., Imran, M. and Ayub, K. "Novel Star-Shaped Benzotriindole-Based Nonfullerene Donor Materials: Toward the Development of Promising Photovoltaic Compounds for High-Performance Organic Solar Cells", Energy Technology, Vol. 10, 2100751, 2022.

[5] Khalid, M., Shafiq, I., Zhu, M., Khan, M.U., Shafiq, Z., Iqbal, J., Alam, M.M., Braga, A.A.C. and Imran, M. "Efficient tuning of small acceptor chromophores with A1-π-A2-π-A1 configuration for high efficacy of organic solar cells via end group manipulation" Journal of Saudi Chemical Society, Vol. 25, 101305, 2021.

[6] Janjua, M.R.S.A., Khan, M.U., Khalid, M., Ullah, N., Kalgaonkar, R., Alnoaimi, K., Baqader, N. and Jamil, S. "Theoretical and conceptual framework to design efficient dye-sensitized solar cells (DSSCs): Molecular engineering by DFT method", Journal of Cluster Science, 32, 243–253, 2021.

[7] Li, W., Chen, M., Cai, J., Spooner, E. L. K., Zhang, H., Gurney, R. S., Liu, D., Xiao, Z., Lidzey, D. G., Ding, L. and Wang, T. "Molecular Order Control of Non-Fullerene Acceptors for High-Efficiency Polymer Solar Cells" Joule, Vol. 3, pp. 819−833, 2019.

[8] Wang, N., Yang, W., Li, S., Shi, M., Lau, T.K., Lu, X., Shikler, R., Li, C.-Z. and Chen, H. "A Non-Fullerene Acceptor Enables Efficient P3HTBased Organic Solar Cells with Small Voltage Loss and Thickness Insensitivity", China Chemistry Letter, Vol. 30, 1277−1281, 2019.

[9] He, C., Yaokai Li, Li, S., Yu, Z., Li, Y., Lu, X., Shi, M., Chang-Zhi Li, C. and Chen, H., "Near-Infrared Electron Acceptors with Unfused Architecture for Efficient Organic Solar Cells", ACS Applied Material and Interfaces, Vol. 12, pp. 16700-16706, 2020.

[10] Gaussian 09, Revision A.02. M. J. Frisch, G. W. Trucks, H. B. Schlegel, P. M. W. Gill, B. G. Johnson, M. A. Robb, J. R. Cheeseman, T. Keith, G. A. Petersson, J. A. Montgomery, K. Raghavachari, M. A. Al-Laham, V. G. Zakrzewski, J. V. Ortiz, J. B. Foresman, C. Y. Peng, P. Y. Ayala, W. Chen, M. W. Wong, J. L. Andres, E. S. Replogle, R. Gomperts, R. L. Martin, D. J. Fox, J. S. Binkley, D. J. Defrees, J. Baker, J. P. Stewart, M. HeadGordon, C. Gonzalez, and J. A. Pople, Gaussian, Inc., Pittsburgh PA, 2009.